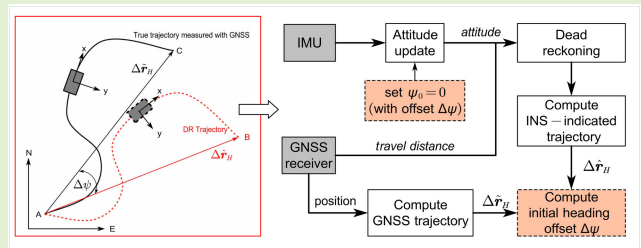


Rapid Initial Heading Alignment for MEMS Land Vehicular GNSS/INS Navigation System

Qijin Chen¹, Huan Lin, Jian Kuang¹, Yarong Luo¹, and Xiaoji Niu¹

Abstract—For the low-cost microelectromechanical system (MEMS) inertial navigation system (INS) and the global navigation satellite system (GNSS)-integrated system in land vehicular applications, quick and accurate coarse alignment is still a challenge, especially for a host vehicle that moves at low speed under low dynamics. In this article, we propose an in-motion coarse initial heading alignment algorithm for the low-cost MEMS INS aided by the GNSS, which is specifically designed for land vehicular conditions. The principle of the proposed method is straightforward when considered in the context of trajectory matching: the MEMS can compute a relative vehicle trajectory through a dead reckoning (DR) calculator using the gyro-derived attitude solution and the travel distance, and the GNSS can provide an absolute vehicle trajectory through its positioning solution. The initial heading is then computed by comparing these DR-indicated and GNSS-indicated trajectories. The proposed algorithm is verified using a civilian vehicle, a wheeled robot, and an agricultural tractor under different motion and dynamic conditions. The results show that the initial heading could be quickly determined with an accuracy of 0.25°, 0.6°, and 1.6° at a 98.6% confidence level within 5 s for the car, robot, and tractor tests, respectively.

Index Terms—Dead reckoning (DR), global navigation satellite system (GNSS)/inertial navigation system (INS) integration, initial alignment, in-motion alignment, land vehicular navigation, microelectromechanical system (MEMS) INS.



I. INTRODUCTION

THE navigation states, including position, velocity, and attitude, must be initialized before an inertial navigation system (INS) can be used to provide a navigation solution. The initial position and velocity can be relatively easy to obtain, e.g., from a global navigation satellite system (GNSS) receiver or other aiding sensors [1], while the attitude initialization, known as alignment, is not that straightforward and requires specific procedures and algorithms. The problem of the alignment for the low-cost microelectromechanical system (MEMS) INS differs from that for the high-grade inertial measurement unit (IMU), since a low-cost MEMS IMU is

not able to measure the Earth's rotation rate with sufficient accuracy due to the large gyro bias [1], [2], [3]. When the INS remains stationary with respect to the Earth, the roll and pitch angles can still be determined through the accelerometer leveling process in a short period even for low-cost MEMS IMUs. Thus, it is the heading angle initialization that poses the major difficulty in the initial alignment for an MEMS INS.

To initialize the heading angle of MEMS INSSs, other external sensors must be employed, such as the GNSS, the Doppler velocity log [4], [5], an odometer [6], and geomagnetic sensors [7]. The GNSS is the most common external aid for INSSs; thus, we focus on the literature reviews of land vehicular INSSs aided by the GNSS. The initial heading can be determined with GNSS assistance either in a direct or indirect manner. In the direct approach, the initial heading can be obtained from the GNSS receiver using a pair of antennas mounted on the same vehicle. However, dual antennas add cost and complexity, and the GNSS heading is noisy, particularly if the baseline between the antennas is short, which is not suitable for a small host vehicle, such as a robot ground vehicle and quadruped robots. When the INS is in motion, the vehicle heading can be determined from the GNSS velocity vector projected in the horizontal plane [7], [8] or determined from the GNSS trajectory [9], [10], [225]. The initial headings

Manuscript received 12 January 2023; revised 17 February 2023; accepted 18 February 2023. Date of publication 28 February 2023; date of current version 31 March 2023. This work was supported in part by the National Natural Science Foundation of China under Grant 41904019. The associate editor coordinating the review of this article and approving it for publication was Prof. Bin Gao. (Corresponding author: Jian Kuang.)

Qijin Chen and Xiaoji Niu are with the GNSS Research Center, Wuhan University, Wuhan 430072, China, and also with the Hubei Luo-jia Laboratory, Wuhan 430079, China (e-mail: chenqijin@whu.edu.cn; xjniu@whu.edu.cn).

Huan Lin, Jian Kuang, and Yarong Luo are with the GNSS Research Center, Wuhan University, Wuhan 430072, China (e-mail: kuang@whu.edu.cn).

Digital Object Identifier 10.1109/JSEN.2023.3247587

from these approaches are usually noisy, and the accuracy of which degrades when the vehicle turns and moves at low speed.

The initial heading can also be determined in an indirect manner by fusing the GNSS and IMU measurements through a Kalman filter or optimization-based approach. The filtering-based methods generally use an appropriate Kalman filter to estimate the initial attitude based on a linearized error model [1], [11], [12], pp. 315–324 or a nonlinear error model considering large heading uncertainty [13], [14]. For example, Shin and El-Sheimy [3] studied the alignment of low-cost IMUs using an unscented Kalman filter, which allows large initial attitude error uncertainty. A field test showed that the initial heading alignment accuracy converges to approximately 0.4° (rms) within 50 s. Han and Wang [1] proposed a two-stage Kalman filtering algorithm for the initial alignment of a low-cost INS aided by the global positioning system (GPS). They reported that 0.3° heading alignment accuracy can be achieved in approximately 150 s. Additional similar extensive studies can be found [14]. These filtering approaches perform well and are able to achieve accurate alignment results but usually require a relatively long period for the filter to converge to a stable estimate.

Wu et al. [15] proposed a recursive optimization-based alignment (OBA) method, which transforms the attitude alignment problem into a continuous attitude determination issue using infinite vector observations [16]. Wu et al. [17] improved this method by jointly estimating the GNSS antenna lever arm (LA) and inertial sensor biases via online optimization. The OBA method provides us an innovative solution to the alignment problem from a brand-new perspective. It was initially developed for the high-grade strapdown INS and performs well with navigation-grade IMUs but may degrade significantly in performance, as the biases of the inertial sensors become larger for the MEMS IMUs we discuss [18]. To extend the OBA method to low-cost INS alignment, a dynamic OBA method [19] that can estimate the gyroscope biases coupled with the attitude was developed, for which Huang et al. [20] developed an efficient implementation. To date, many variants of the OBA method and follow-up studies that attempted to improve its performance and extend its application scope can be found; for a summary, see [21]. Zhang et al. [22] extended the velocity-based OBA method to the navigation of a low-speed agricultural tractor, reporting 4° heading alignment accuracy within 60 s using a MEMS INS.

The characteristics of the mentioned indirect in-motion alignment through filtering or optimization-based methods can be summarized as follows: 1) they perform well and can be used in a variety of applications but usually take a relatively long period, for example, approximately 50 s at minimum, to converge to a stable initial heading estimate for MEMS INSs and 2) they generally require the host vehicle to perform sufficient maneuvering and dynamic motion, for example, a change in acceleration, to achieve the best performance. Currently, an increasing number of land vehicular navigation applications using MEMS INSs, such as autonomous driving and UAVs, require the system to have the quick restart capability [23]. The initial heading alignment of a low-cost MEMS INS is

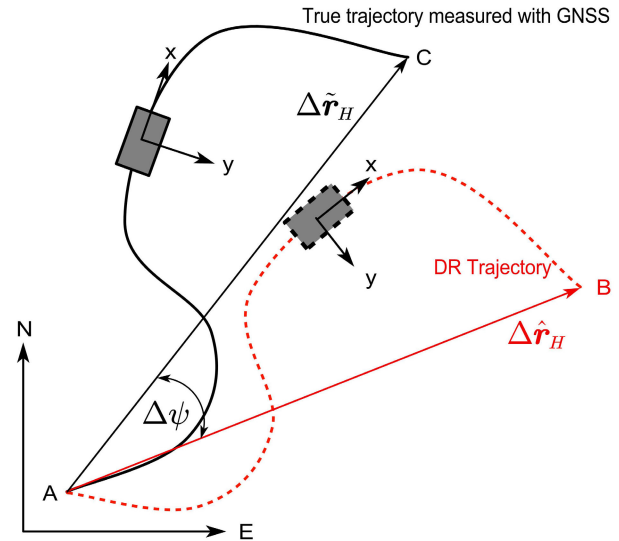


Fig. 1. Illustration of the proposed INS initial heading alignment principle. The DR- and GNSS-indicated trajectories are similar in shape in the horizontal plane due to the initial heading offset $\Delta\psi$ to be determined.

still difficult to acquire, especially for a host vehicle that moves at low speed and under low dynamics. There remains an urgent need for a quick and accurate initial heading alignment method.

Motivated by the above technical challenges and application demands, we propose a new INS alignment method specific for land vehicle applications, which is able to accurately determine the initial heading in a short time. The principle of the proposed method is straightforward: the MEMS INS computes a relative vehicle trajectory through a dead reckoning (DR) calculator using the gyro-derived attitude solution and the travel distance without using the accelerometer triads, and the GNSS provides an absolute vehicle trajectory through its positioning solution. The initial heading is then computed by comparing the DR-indicated and GNSS-indicated trajectories. The proposed method differs from previous approaches in the following ways: 1) the initial heading can be determined, for example, accurate to 0.25° , in 5 s, which is much more time efficient than the existing method and 2) the proposed method has few requirements on the host vehicle dynamics; i.e., it does not require the vehicle to move with a change in acceleration, to ensure accuracy convergence. The proposed algorithm is validated using a civilian vehicle, a wheeled robot, and a farm tractor under different motion and dynamic conditions.

II. METHODOLOGY

Fig. 1 illustrates the basic principle of the proposed initial heading alignment method. The host vehicle moves on the ground to collect IMU and GNSS data. Then, the initial heading alignment principle is quite straightforward.

- 1) The initial heading angle of the IMU is assumed to be zero to start a DR calculator to compute the vehicle trajectory using the gyro-derived attitude and the travel distance calculated from the GNSS positions. We call this resulting trajectory the DR-indicated trajectory.

- 2) The actual trajectory of the vehicle can also be measured with the GNSS, which we call the GNSS-indicated trajectory.
- 3) The horizontal DR-indicated trajectory can be regarded as having undergone a rotation with respect to the true trajectory; thereby, the offset of the assumed initial heading angle in step 1, denoted by $\Delta\psi$, can be determined by comparing the DR- and GNSS-indicated trajectories to accomplish the initial heading alignment.

The proposed initial heading alignment for the land vehicular navigation application is established on such a nonholonomic constraint (NHC [24]) assumption.

Assumption 1: The movement of the host vehicle conforms to the NHC, indicating that the land vehicle motion is constrained, where the vehicle can move only in the longitudinal direction, and the velocity in the plane perpendicular to the longitudinal direction is almost zero.

A. Principle of the Proposed Heading Alignment Method

The vehicle velocity measurement from an odometer is usually referenced for the v-frame, which is then transformed into the n-frame by the following transformation:

$$\mathbf{v}^n = \mathbf{C}_b^n \mathbf{C}_v^b \mathbf{v}^v \quad (1)$$

where the superscript n refers to the north–east–down navigation coordinate frame (the n-frame), b denotes the IMU body frame in which the accelerations and angular rates generated by the strapdown accelerometers and gyroscopes are resolved (the b-frame), and v is the forward–outward–downward vehicle frame (the v-frame); the vehicle-referenced velocity \mathbf{v}^v has a nonzero value v for the first element and a value of zero for the other elements, i.e., $\mathbf{v}^v = [v \ 0 \ 0]^T$. \mathbf{C}_b^n denotes the direction cosine matrix that transforms vectors from the b-frame to the n-frame. \mathbf{C}_v^b is the direction cosine matrix that transforms vectors from the v-frame to the b-frame, which results from the misalignment angles of the IMU with respect to the host vehicle.

Remark 1: In this research, we assume that the axes of the IMU are aligned with the axes of the v-frame; thus, the matrix \mathbf{C}_v^b is the identity matrix, i.e., $\mathbf{C}_v^b = \mathbf{I}$. This assumption is reasonable, since according to our previous research [25], the mounting angles can be estimated with sufficient accuracy in advance.

Therefore, (1) is simplified as follows:

$$\mathbf{v}^n = \mathbf{C}_b^n \mathbf{v}^v = \mathbf{C}_b^n \mathbf{v}^b. \quad (2)$$

The travel distance of the vehicle derived from the GNSS trajectory or measured by an odometer is also referenced to the v-frame, and considering remark 1, we have

$$\Delta \mathbf{s}^b(t) = \int_0^t \mathbf{v}^v(\tau) d\tau = \int_0^t \mathbf{v}^b(\tau) d\tau. \quad (3)$$

$\Delta \mathbf{s}^b$ also has a nonzero value for the first element Δs and a value of zero for the other elements; i.e., $\Delta \mathbf{s}^b(t) = [\Delta s(t), 0, 0]^T$.

The DR position vector is updated by numerically integrating the geographic velocity components as follows:

$$\mathbf{r}(t) = \mathbf{r}(0) + \mathbf{D}_R^{-1} \Delta \mathbf{r}^n(t) \quad (4)$$

$$\Delta \mathbf{r}^n(t) = \int_0^t \mathbf{C}_b^n(\tau) \mathbf{v}^b(\tau) d\tau \quad (5)$$

where $\mathbf{r}(t)$ and $\mathbf{r}(0)$ are the curvilinear position vectors at time t and t_0 , respectively. $\Delta \mathbf{r}^n = [\Delta r_N \ \Delta r_E \ \Delta r_D]^T$ is the position increment vector, i.e., the delta position vector from t_0 to t , resolved in the n-frame. The matrix $\mathbf{D}_R^{-1} = \text{diag}([(1/R_M + h) \ (1/(R_N + h) \cos \varphi) \ -1]^T)$ is a diagonal matrix that converts the position increment vector in the n-frame in meters to the delta latitude and delta longitude in radians.

The attitude matrix $\mathbf{C}_b^n(t)$ at time t in (5) is updated as follows using the direction cosine matrix product chain rule [16]:

$$\mathbf{C}_b^n(t) = \mathbf{C}_{b(t)}^{n(t)} = \mathbf{C}_{n(0)}^{n(t)} \mathbf{C}_{b(0)}^{n(0)} \mathbf{C}_{b(t)}^{b(0)} \quad (6)$$

where the attitude matrices $\mathbf{C}_{b(t)}^{b(0)}$ and $\mathbf{C}_{n(0)}^{n(t)}$ account for the attitude changes of the b-frame and n-frame, respectively, between time t_0 and t . $\mathbf{C}_{b(0)}^{n(0)}$ is the constant initial attitude matrix to be determined during alignment. Because the proposed method can accomplish the alignment in only a few seconds with several meters of movement, the change in the n-frame's orientation is negligibly small, i.e., $\mathbf{C}_{n(0)}^{n(t)} \approx \mathbf{I}$. Thus, we have

$$\mathbf{C}_b^n(t) \approx \mathbf{C}_{b(t)}^n = \mathbf{C}_{b(0)}^n \mathbf{C}_{b(t)}^{b(0)} \quad (7)$$

where $\mathbf{C}_{b(0)}^n$ is the initial attitude matrix. Equation (6) updates the attitude matrix \mathbf{C}_b^n based on $\mathbf{C}_{b(t)}^{b(0)}$ to account for the angular rate of the b-frame with respect to nonrotating space [26]. $\mathbf{C}_{b(t)}^{b(0)}$ is calculated by integrating the gyro measurements. The errors contained in the computed matrix $\hat{\mathbf{C}}_b^n$ come from both the error in $\hat{\mathbf{C}}_{b(0)}^n$ and the computed $\hat{\mathbf{C}}_{b(t)}^{b(0)}$. Thus, we have

$$\hat{\mathbf{C}}_b^n(t) = \hat{\mathbf{C}}_{b(0)}^n \hat{\mathbf{C}}_{b(t)}^{b(0)} \quad (8)$$

where $\hat{\cdot}$ denotes the computed variable.

Remark 2: Since the proposed method can accomplish the alignment process in only a few seconds, the error in $\hat{\mathbf{C}}_{b(t)}^{b(0)}$ can be proven to be negligibly small compared with the error in $\hat{\mathbf{C}}_{b(0)}^n$.

The proof mentioned in remark 2 is given in error analysis. Now, we focus on the matrix $\hat{\mathbf{C}}_{b(0)}^n$. We can assign the angular misalignment error to an error in the n-frame relative to the b(0)-frame without loss of generality [27, pp. 3–78]. Thus, $\hat{\mathbf{C}}_{b(0)}^n$ can be computed as follows:

$$\hat{\mathbf{C}}_{b(0)}^n \triangleq \hat{\mathbf{C}}_{b(0)}^{\hat{n}} = \mathbf{C}_{\hat{n}}^{\hat{n}} \mathbf{C}_{b(0)}^{b(0)} \quad (9)$$

where $\mathbf{C}_{\hat{n}}^{\hat{n}}$ is the direction cosine matrix that transforms vectors from the error-free \hat{n} -frame to the misaligned \hat{n} -frame. The errors contained in $\mathbf{C}_{\hat{n}}^{\hat{n}}$ stem from the errors in the initial Euler angles, since the proposed alignment method initializes the roll and pitch angles through an accelerometer leveling procedure and initializes the INS heading by entering 0° to start the

navigator. As discussed in our previous research [8], even for a MEMS IMU, the roll and pitch angles could be determined within a short static period through the accelerometer leveling procedure, whose error is notably smaller than that of the arbitrarily entered initial heading. Therefore, $\mathbf{C}_n^{\hat{n}}$ can be approximated according to the conversion from Euler angles to the attitude matrix [27, pp. 3–33] as follows:

$$\mathbf{C}_n^{\hat{n}} \approx \begin{bmatrix} \cos \Delta\psi & -\sin \Delta\psi & 0 \\ \sin \Delta\psi & \cos \Delta\psi & 0 \\ 0 & 0 & 1 \end{bmatrix}. \quad (10)$$

Considering remark 2 again, (8) can be approximated by substituting (9) as follows:

$$\hat{\mathbf{C}}_b^n(t) = \mathbf{C}_n^{\hat{n}} \mathbf{C}_{b(0)}^n \mathbf{C}_{b(t)}^{b(0)}. \quad (11)$$

Substituting (7) into (5) yields

$$\Delta \mathbf{r}^n(t) = \int_0^t \mathbf{C}_{b(0)}^n \mathbf{C}_{b(\tau)}^{b(0)} \mathbf{v}^b(\tau) d\tau. \quad (12)$$

The computed delta position vector is obtained as follows:

$$\Delta \hat{\mathbf{r}}^n(t) = \mathbf{C}_n^{\hat{n}} \int_0^t \mathbf{C}_{b(0)}^n \mathbf{C}_{b(\tau)}^{b(0)} \mathbf{v}^b(\tau) d\tau. \quad (13)$$

Substituting (12) into the above equation yields

$$\Delta \hat{\mathbf{r}}^n(t) = \mathbf{C}_n^{\hat{n}} \Delta \mathbf{r}^n(t). \quad (14)$$

By substituting (10) into (14) and retaining the first two components, i.e., the horizontal coordinate components, we have

$$\begin{bmatrix} \Delta \hat{r}_N(t) \\ \Delta \hat{r}_E(t) \end{bmatrix} = \begin{bmatrix} \cos \Delta\psi & -\sin \Delta\psi \\ \sin \Delta\psi & \cos \Delta\psi \end{bmatrix} \begin{bmatrix} \Delta r_N(t) \\ \Delta r_E(t) \end{bmatrix} \quad (15)$$

where $\Delta \hat{r}_N$ and $\Delta \hat{r}_E$ are the north and east components, respectively, of the computed incremental position $\Delta \hat{\mathbf{r}}^n$. Δr_N and Δr_E denote the error-free north and east components of the incremental position $\Delta \mathbf{r}^n$, respectively. We denote $\Delta \hat{\mathbf{r}}_H^n = [\Delta \hat{r}_N \ \Delta \hat{r}_E]^T$ and $\Delta \mathbf{r}_H^n = [\Delta r_N \ \Delta r_E]^T$ as the DR-indicated and true horizontal delta position vectors, respectively, at arbitrary time epoch t . Equation (15) explicitly implies the following.

Remark 3: The DR-indicated trajectory $\Delta \hat{\mathbf{r}}^n(t)$ is similar to the true trajectory measured with the GNSS in shape but with a constant rotation due to the occurrence of the initial heading offset $\Delta\psi$. The DR and GNSS position measurements thereby make $\Delta\psi$ observable.

Therefore, the initial heading bias $\Delta\psi$ could be calculated as follows:

$$\cos \Delta\psi = \frac{\Delta \hat{\mathbf{r}}_H^n \cdot \Delta \mathbf{r}_H^n}{|\Delta \hat{\mathbf{r}}_H^n| |\Delta \mathbf{r}_H^n|} \quad (16)$$

where $|\Delta \hat{\mathbf{r}}_H^n|$ and $|\Delta \mathbf{r}_H^n|$ are the lengths of vectors $\Delta \hat{\mathbf{r}}_H^n$ and $\Delta \mathbf{r}_H^n$, respectively. The above equation is the basic principle of the determination of the initial heading of the proposed alignment method.

B. Algorithm Implementation

The attitude is updated from the start time epoch by integrating the gyro measurement using the direction cosine matrix chain rules [26] as follows:

$$\mathbf{C}_{b(k)}^{n(k)} \approx \mathbf{C}_{b(k)}^n = \mathbf{C}_{b(k-1)}^n \mathbf{C}_{b(k)}^{b(k-1)} \quad (17)$$

$$\mathbf{C}_{b(k)}^{b(k-1)} = \mathbf{I}_3 + \sin \phi_k (\mathbf{u}_k \times) + (1 - \cos \phi_k) (\mathbf{u}_k \times)^2 \quad (18)$$

$$\phi_k = \Delta \theta_k + \frac{1}{12} \Delta \theta_{k-1} \times \Delta \theta_k \quad (19)$$

where k denotes the time instant t_k , \mathbf{I}_3 is the 3×3 identity matrix, ϕ_k is the rotation vector defining the frame b_k attitude relative to the frame b_{k-1} at time t_k , ϕ_k is the length of ϕ_k , \mathbf{u}_k is the unit rotation vector along ϕ_k , and $\Delta \theta_{k-1}$ and $\Delta \theta_k$ are the incremental angle measurements of the IMU at t_{k-1} and t_k , respectively.

The DR position is updated by numerically integrating the geographic velocity components as follows:

$$\mathbf{r}_k = \mathbf{r}_{k-1} + \mathbf{D}_R^{-1} \mathbf{C}_{b(t_{k-1})}^n \Delta \mathbf{s}_k^b \quad (20)$$

where \mathbf{r}_{k-1}^n and \mathbf{r}_k^n are the curvilinear position vectors at t_{k-1} and t_k , respectively. The delta position vector required in (15) can be calculated as follows:

$$\Delta r_N = \Delta \varphi (R_M + h) \quad (21)$$

$$\Delta r_E = \Delta \lambda (R_N + h) \cos \varphi \quad (22)$$

where $\Delta \varphi$ and $\Delta \lambda$ denote the change in latitude and longitude, respectively. R_M and R_N are the radii of curvatures along lines of constant longitude and latitude, respectively. The proposed alignment algorithm is implemented according to Algorithm 1.

In the implementation, the initial heading can be determined by using either one single sample of the simultaneous observation vectors $\Delta \hat{\mathbf{r}}_H^n$ and $\Delta \mathbf{r}_H^n$ or multiple samples available in the alignment period. If multiple samples are incorporated in the alignment calculation, the solution of the initial heading could be obtained with the least squares estimator. According to our experience, if the alignment is accomplished in a short period of time, there is no significant improvement using multiple samples compared with that achieved using the longest vector.

III. ERROR ANALYSIS

As illustrated in Fig. 1, the initial heading is determined by comparing the azimuth of the DR-indicated delta position vector $\Delta \hat{\mathbf{r}}_H^n$ and the GNSS-indicated delta position vector $\Delta \tilde{\mathbf{r}}_H^n$. Thus, the heading alignment accuracy is influenced by both the DR-indicated and GNSS-indicated trajectories. The azimuth or heading errors of the DR-indicated and GNSS-indicated delta position vectors can be computed in a straightforward manner, as follows:

$$\delta \psi_I = \frac{\delta \Delta \hat{\mathbf{r}}_{H,T}}{|\Delta \mathbf{r}_H^n|} \quad (23)$$

$$\delta \psi_G = \frac{\delta \Delta \tilde{\mathbf{r}}_{H,T}}{|\Delta \mathbf{r}_H^n|} \quad (24)$$

where $\delta\psi_I$ is the azimuth error of the DR-indicated vector $\Delta\hat{\mathbf{r}}_H$ caused by the errors in the gyro-derived attitude; $\delta\psi_G$ is the azimuth error of the vector $\Delta\tilde{\mathbf{r}}_H^n$ due to the GNSS position errors. $\delta\Delta\hat{\mathbf{r}}_{H,T}$ and $\delta\Delta\tilde{\mathbf{r}}_{H,T}$ denote the transversal error component of the vector $\Delta\hat{\mathbf{r}}_H$ and $\Delta\tilde{\mathbf{r}}_H$, respectively; $|\Delta\mathbf{r}_H^n|$ is the length of the true delta position vector, i.e., \mathbf{r}_{AC} in Fig. 1. It is explicit from (23) and (24) that for a given travel distance $|\Delta\mathbf{r}_H^n|$, the more accurate $\Delta\hat{\mathbf{r}}_H^n$ and $\Delta\tilde{\mathbf{r}}_H^n$ are, the more accurate the initial heading should be. In contrast, the heading alignment error is inversely proportional to the travel trajectory length.

Neglecting the correlation between $\delta\psi_I$ and $\delta\psi_G$, the heading error induced by them can be analyzed independently, and the final heading alignment error can be computed according to the error propagation law as follows:

$$\sigma_\psi = \sqrt{\sigma_{\psi,I}^2 + \sigma_{\psi,G}^2} \quad (25)$$

where σ_ψ denotes the root mean square error (RMSE) of the heading alignment results, and $\sigma_{\psi,I}$ and $\sigma_{\psi,G}$ are the RMSEs of $\delta\psi_I$ and $\delta\psi_G$, respectively. In the following, we analyze the gyro-derived attitude errors and their ensuing impact on the alignment accuracy, and then evaluate the alignment uncertainty caused by the GNSS positioning errors.

A. Impacts of the Gyro-Derived Attitude Error on Alignment

DR positioning accuracy is known to be influenced by attitude and travel distance measurement. Since precise GNSS can accurately determine the track distance, the gyro-derived attitude errors are the main error sources of the DR-indicated delta position vectors. According to the detailed analysis in

Algorithm 1 Initial Heading Alignment of the MEMS INS for Land Vehicular Applications

Input: $\mathbf{r}_{\text{GNSS}}(t_{k-1})$, $\mathbf{r}_{\text{GNSS}}(t_k)$, \mathbf{r}_0 , \mathbf{r}_{k-1} , $\mathbf{C}_b^n(t_{k-1})$, $\Delta\theta_{k-1}$, $\Delta\theta_k$

Calculation of the DR position \mathbf{r}_k :

- 1: Compute $\Delta\varphi$, $\Delta\lambda$ between the GNSS positioning solutions $\mathbf{r}_{\text{GNSS}}(t_{k-1})$ and $\mathbf{r}_{\text{GNSS}}(t_k)$.
- 2: Compute the delta distance $\Delta s_k = \sqrt{\Delta r_E^2 + \Delta r_N^2}$ using (21) and (22).
- 3: Compute $\Delta s_k^b = [\Delta s_k \ 0 \ 0]^T$
- 4: Compute the current DR position vector \mathbf{r}_k using (20).

Calculation of $\Delta\hat{\mathbf{r}}_H^n$ and $\Delta\mathbf{r}_H^n$:

- 5: Compute the DR-indicated delta position vector $\Delta\hat{\mathbf{r}}_H^n$ between \mathbf{r}_k and \mathbf{r}_0 using (21) and (22).
- 6: Compute the GNSS-indicated delta position vector $\Delta\mathbf{r}_H^n$ between $\mathbf{r}_{\text{GNSS}}(t_k)$ and \mathbf{r}_0 using (21) and (22).

Calculation of $\mathbf{C}_b^n(t_k)$:

- 7: Update the gyro-derived attitude matrix $\mathbf{C}_b^n(t_k)$ based on $\mathbf{C}_b^n(t_{k-1})$, $\Delta\theta_{k-1}$ and $\Delta\theta_k$ using (17)-(19).

Calculation of $\Delta\psi$:

- 8: Compute $\Delta\psi$ based on the computed $\Delta\hat{\mathbf{r}}_H^n$ and $\Delta\mathbf{r}_H^n$ using equation (16).

Output: $\Delta\psi$, $\mathbf{C}_b^n(t_0)$, \mathbf{r}_k , $\mathbf{C}_b^n(t_k)$.

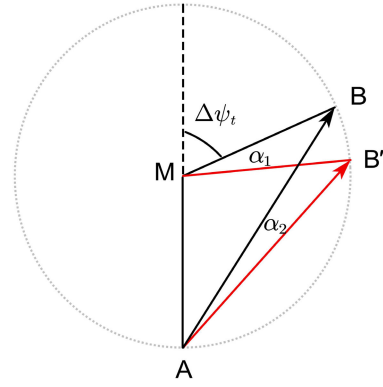


Fig. 2. Illustration of the gyro scale factor error on the final heading alignment accuracy.

the Appendix, the impacts of the random noise and fixed gyro bias on gyro-derived attitude can be safely ignored as long as the alignment is accomplished in a short time. The impact of the gyro scale factor error on the final alignment accuracy needs to analyze in detail.

The gyro-derived heading error is not the final impact on the alignment, since the attitude error is integrated with the travel distance to produce a positioning error of the endpoint. For the most general case, we assume that the vehicle moves along the trajectory \overline{AMB} , as depicted in Fig. 2, and turns a $\Delta\psi_t$ angle at the middle point of the path. In this figure, A and B are the start and end points of the DR-indicated trajectory, and M is the middle of the trajectory. Then, the gyro scale factor error would cause a heading drift α_1 proportional to the steering angle and finally lead to an error in the azimuth of the DR-indicated delta position vector $\overline{AB'}$, i.e., α_2 . It is explicit from this figure that $\alpha_2 = (1/2)\alpha_1$, because the central angle is always twice of any inscribed angle subtended by the same arc. Suppose that in the worst cases, the vehicle turns an angle of 50° during alignment; then, the error of gyro-derived heading is $\alpha_1 = \delta\psi_{b,sf} = 0.25^\circ$ as discussed in Appendix (A.4). The ensuing error in the final heading alignment will be $\alpha_2 = 0.5\alpha_1 = 0.125^\circ$.

B. Impacts of the GNSS Positioning Error on Alignment

Equation (24) illustrates that it is the relative positioning errors between two epochs that actually influence the accuracy. The real time kinematic (RTK) GNSS is known to be accurate to 2 cm (RMSE) in the horizontal direction, but the relative positioning between two epochs within 5 s is accurate to about 1 mm according to our previous research [28]. If the host vehicle moves 5 m forward, i.e., the travel distance, during the alignment period, then we have $\delta\psi_G = 0.001/5 \text{ rad} \approx 0.01^\circ$. It should be noted that this is a statistic value; in real individual case, the relative positioning may not be so accurate due to, for example, the multipath effect.

For the single point positioning (SPP), the relative positioning accuracy is about 0.3 m within 5 and 20 s in both the east and north directions [28]. If the SPP solution is used as the reference trajectory and the vehicle also moves a distance of 5 m, the resulting GNSS trajectory-indicated heading error is about $\delta\psi_G = 0.3/5 \text{ rad} \approx 3.4^\circ$. If the trajectory length is 20 m, then the heading error is reduced to $\delta\psi_G = 0.3/20 \text{ rad} \approx 0.8^\circ$.

Therefore, when the reference trajectory is measured with GNSS SPP, a longer trajectory is needed to achieve acceptable accuracy.

It should be noted that the given alignment period length, i.e., 5 s, is an empirical value. This value is determined by the following two factors: 1) the proposed alignment should be finished in as short a time as possible to realize rapid alignment and 2) favorable alignment accuracy should be achieved in this short time period. The selection of this value should ensure that the vehicle's travel distance is long enough, so that the GNSS-indicated error represented by formula (24) is smaller than or close to the INS-indicated error represented by formula (23). For vehicle-mounted RTK/INS-integrated navigation, 5 s is long enough (this is also related to the vehicle speed), because the positioning error of RTK is small, and increasing the alignment time will not improve the alignment accuracy. But for SPP, due to its larger positioning error, in order to control the influence of GNSS-indicated errors, the delta position vector must be increased, and the alignment time generally needs to be increased to 20 s, which will be discussed in Section IV-C.

C. Expected Alignment Accuracy

Full determination of the alignment error through a theoretical approach is too complex, since the alignment accuracy is also affected by the host vehicle trajectory and dynamics. Thus, we roughly compute the expected alignment accuracy by case study. Suppose the typical MEMS IMU used in our field test, as listed in Table II, is fixed on a host vehicle that conforms to the NHC and travels at a low speed of 1 m/s, and suppose the alignment is accomplished in a short period of time, e.g., 5 s.

Case 1: The vehicle travels in a straight line, and GNSS RTK is used as aiding. Under this condition, the impact of the gyro's random noise, scale factor, and cross coupling is all negligibly small. The GNSS-induced heading is accurate to 0.02° ; thus, the joint impact of the gyro and GNSS is $\sigma_\psi \approx 0.02^\circ$ according to (25).

Case 2: The vehicle travels in a straight line, and GNSS SPP is used as aiding. The impact of the gyro's sensor errors is the same as in case 1, and the GNSS positioning error becomes the main error source, whose impact can be as large as 3.4° when the vehicle travels a distance of 5 m, as analyzed previously. Increasing the travel distance would improve the alignment accuracy.

Case 3: The vehicle turns around during alignment, and RTK is used as aiding. The impact of the gyro's random noise and GNSS positioning error is the same as in case 1, but the impact of the gyro's scale factor error increases significantly.

Case 4: The vehicle turns around during alignment, and SPP is used as aiding. Under this condition, the alignment error is mainly due to the joint impact of the gyro's scale factor and GNSS positioning errors, which can be computed by (25).

IV. EXPERIMENTS AND RESULTS

The proposed method is verified using three different types of land vehicles under different conditions, as shown in Fig. 3.

A self-developed MEMS GNSS/INS-integrated system, named INS-Probe, was used to collect raw IMU data to test the proposed method. In this system, a MEMS IMU-ADIS16460 from Analog Devices Inc. (ADI) was integrated and synchronized with a built-in GNSS receiver card from u-blox. GNSS receivers of high quality from NovAtel Inc. were employed to collect raw GNSS observations. Table I lists the important information on the collected datasets and the key instrument used in the field tests.

For the civilian vehicle test, the car followed a closed path under open-sky conditions, as depicted in Fig. 4 (top). The course contained sufficient straight and curved sections, which allowed us to evaluate the performance of the proposed method under different dynamic maneuvers. The vehicle retraced this track many times to collect three independent groups of datasets, each covering approximately 0.8 h. The baseline length between the rover receiver and base station did not exceed 15 km. Similar experiments were conducted on a wheeled robot under open-sky conditions on a campus playground at Wuhan University. The travel course is depicted in Fig. 4 (bottom). The baseline length between the rover receiver and the base station was approximately 300 m. Two independent groups of datasets were collected. Experiments on a tractor were carried out in November 2016. In this test, a NovAtel GNSS receiver with a pair of antennas was used to provide an independent heading reference. Two independent groups of datasets were collected. The moving trajectory and more details on the experiment can be found in our previous work [22] and in Tables I and II.

A. Data Processing

The raw GNSS data from the master and rover receivers were processed in the carrier-phase-based differential positioning mode in forward filtering, just as the RTK positioning works to provide 1-Hz RTK positioning solutions. Then, the resulting GNSS positioning solution and the raw IMU data in each group were divided into small segments, each covering 5 s, to perform the independent alignment using the proposed algorithm. It should be noted that although we validated the algorithm by processing the collected data, the algorithm could be implemented in a real-time manner. The data processing procedure is described below.

- 1) Set the alignment period to 5 s, and then extract 5-s length synchronous data segments from the raw IMU data of INS-Probe and the GNSS positioning results.
- 2) Perform initial heading alignment based on the dataset from step 1 using the proposed algorithm as depicted in Algorithm 1.
- 3) Compare the initial heading alignment results from step 2 with the qualitative independent reference to compute the heading alignment error of this individual sample.
- 4) Repeat step 1 and move forward to extract a new data segment, and repeat steps 2 and 3 to obtain the next alignment sample.
- 5) Repeat steps 1–4 until the end of one dataset is reached.
- 6) Repeat steps 1–5 to evaluate the performance in different runs of the car, robot, and tractor.

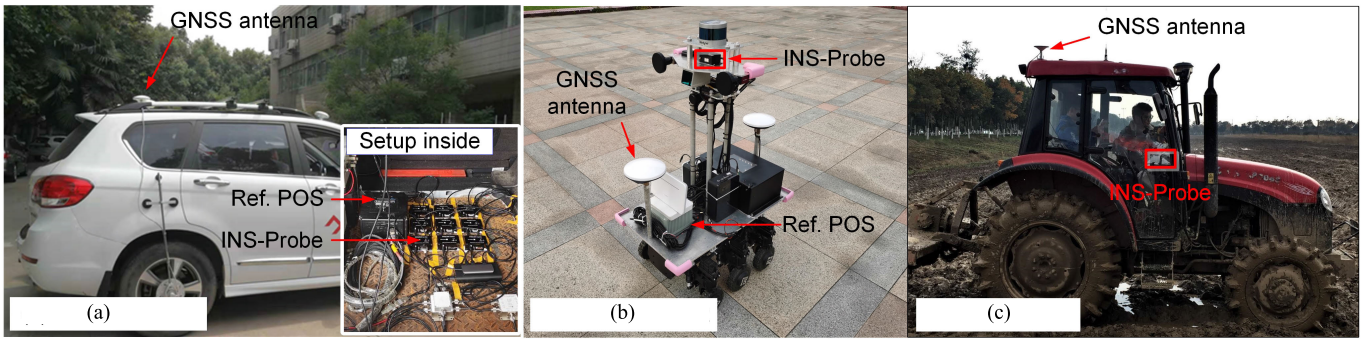


Fig. 3. Experimental setups for different type of vehicles, including (a) civilian vehicle, (b) wheeled robot, and (c) farm tractor.

TABLE I
BRIEF INFORMATION ON THE COLLECTED DATASETS AND KEY INSTRUMENT IN THE FIELD TESTS

	Civilian vehicle	Wheeled robot	Farm tractor
Data length	3 groups, 2.4 h	2 groups, 1.4 h	2 groups, 2.6 h
Speed	15 m/s	1.5 m/s	1.2 m/s
Key instrument	<ul style="list-style-type: none"> test IMU: INS-Probe base and rover GNSS receiver: NovAtel OEM-7 receivers heading reference: from POS-A15, accurate to 0.01° (RMSE) 	<ul style="list-style-type: none"> test IMU: INS-Probe base and rover GNSS receiver: NovAtel OEM-7 receivers heading reference: from POS-620, accurate to 0.01° (RMSE) 	<ul style="list-style-type: none"> test IMU: INS-Probe rover receiver: NovAtel OEM-7 receivers heading reference: dual antenna, accurate to 0.08° (RMSE)

TABLE II
SPECIFICATIONS OF THE KEY INSTRUMENT

INS-Probe	MEMS IMU: ADIS16460 gyroscope in-run bias instability: $8^\circ/h$ accelerometer in-run bias stability: 200 mGal data rate: 200 Hz
POS-A15 & POS620	navigation-grade POS gyroscope in-run bias stability: $0.01^\circ/h$ accelerometer in-run bias stability: 10 mGal data rate: 200 Hz
GNSS receiver	NovAtel OEM-7 data rate: 1 Hz RTK performance: 10 mm + 1 ppm RMS

B. Results

Fig. 5 plots the errors of the first 1000 independent alignment samples of group 1 from the car, robot, and tractor tests, respectively. Fig. 6 depicts the cumulative distribution function (CDF) plots of the initial heading errors from different tests. These plots reveal that the initial heading could be determined with an accuracy of 0.25° , 0.6° , and 1.6° at a 98.6% confidence level within only 5 s for the car, robot, and tractor tests, respectively. The CDF plots from different groups of datasets for the same application show good consistency, which proves the feasibility and robustness of the approach to a certain extent. Zhang et al. [22] reported that the initial heading alignment accuracy converges to 4° in 60 s for the velocity-based OBA method using the same tractor data. Huang et al. [20] compared the mainstream in-motion

alignment methods for the MEMS GNSS/INS-integrated system and showed that the best performance of the previous method was a 2° heading alignment accuracy in approximately 75–100 s. Comparing our result with those previous research, we can conclude that the proposed alignment method performs much better in terms of both alignment accuracy and time efficiency.

Returning back to Fig. 5 and upon closer observation of the top panel for the land vehicle tests, we notice that the alignment errors of some samples, for example, samples 200 and 400, are significantly larger than others. We find that these samples always appeared as the host vehicle turned around, and the alignment accuracy was recovered once the vehicle began traveling in a straight line again. To explicitly illustrate this issue, we plot the alignment errors together with the steering rate $\omega_{ib,z}$ and the speed of the host vehicle, as shown in Fig. 7. Clearly, the alignment errors highly correlate with the change rate of the vehicle's heading angle, and the alignment accuracy decreases as $\omega_{ib,z}$ increases, i.e., as the vehicle turns around. The vehicle speed also slowed down with the heading steerings, which might be another reason for the alignment degradation.

The reasons for the decrease in alignment accuracy when the host vehicle turns around are most likely threefold: 1) the influence of the gyro's scale factor error becomes much more significant when the vehicle turns around; 2) the travel distance in the alignment period decreases as the vehicle slows down, which leads to a shorter delta position vector Δr_H^n in (16), thus resulting in larger alignment errors; and 3) the influence of the NHC LA error, and the NHC condition violates when

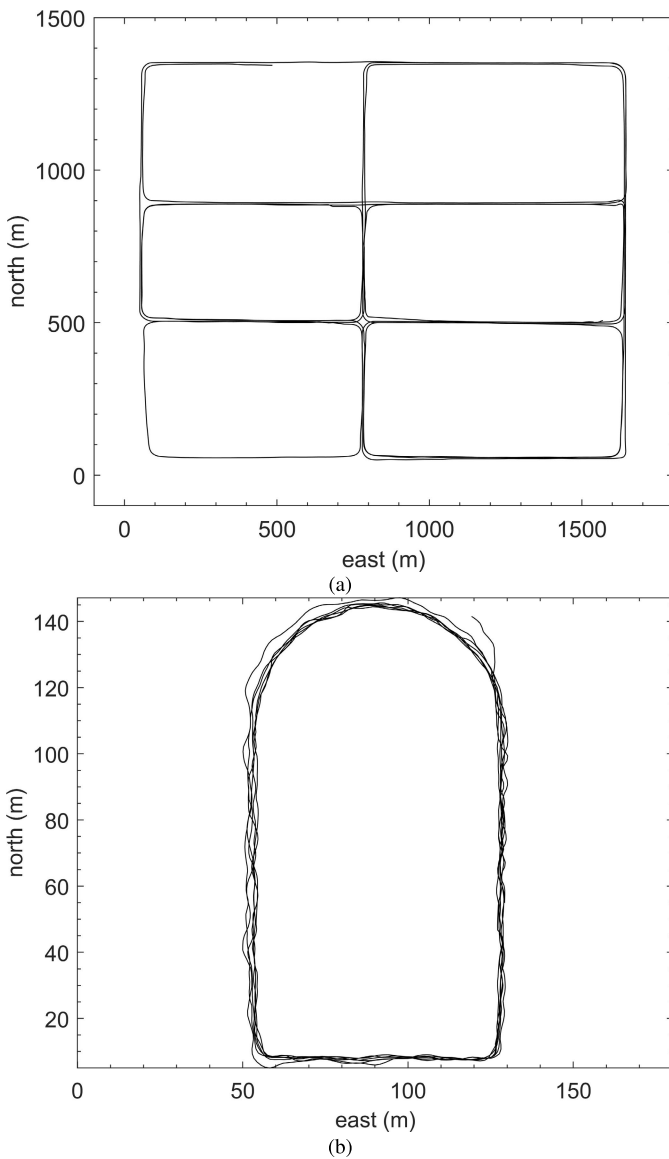


Fig. 4. Ground courses of (a) civilian land vehicle and (b) wheeled robot.

the vehicle turns. We verify and comment on these possible reasons one by one in the following.

In Fig. 8, we evaluate the influence of the gyro's scale factor error by using the dataset of group 1 from the car test as an example. In this figure, the results without compensation are the same as those shown in Fig. 5 (top), and we plot only the first 700 samples to make the curves easier to read. It should be noted that the compensated gyro scale factor was about 0.2%, estimated using the entire dataset through an independent RTK/INS integration filter in postprocessing. In practice, the scale factor error cannot be estimated within such a short alignment period due to the lack of observability; thus, we have to accept these errors at full magnitude. Fortunately, from this comparison, we find that the contribution of the gyro's scale factor error is not as significant as expected even when azimuth change reaches 50° during alignment. Returning back to Fig. 7, we notice larger alignment errors around alignment samples 844 and 890, but there are no

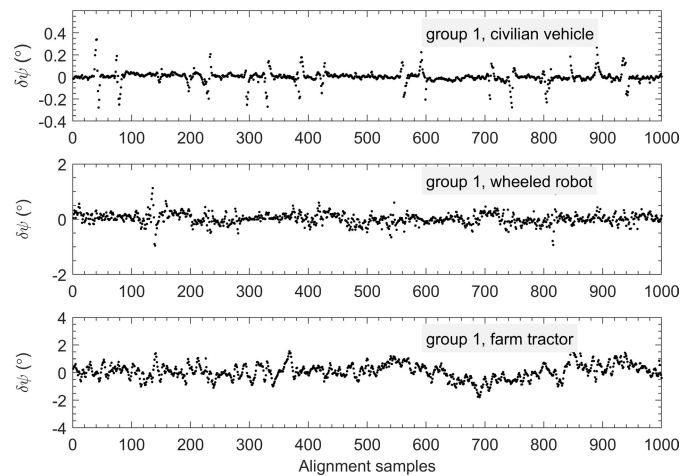


Fig. 5. Typical initial heading alignment errors from group 1 in the tests.

significant heading rotation rates when the vehicle travels at low speed. This occurs because the lower speed leads to a shorter travel distance vector and, thus, causes larger alignment errors.

Fig. 9 shows the influence of the NHC LA, which refers to the vector from the IMU measurement center to the NHC valid point, which is typically assumed as the middle point of the rear axle. In this test, we accurately measured NHC LA vector, while as a comparison, we intentionally disable the NHC LA compensation to see its impact. From this comparison, we find that the NHC LA has significant influence on the alignment accuracy when the vehicle turns around, because the heading and trajectory no longer coincide when the vehicle is turning around [10, p. 225]. In practice, we suggest measuring the NHC LA accurate to approximately 2 cm before applying the proposed alignment algorithm. However, it is impossible for us to compensate exactly for the effect of the NHC LA, because the NHC LA may vary in size when the vehicle undergoes different steering angle and different dynamics.

C. Discussion

We notice that even after compensating for the effect of the gyro scale factor and the NHC LA, the proposed method cannot achieve the same accuracy when the vehicle turns around as that when it travels along a straight-line path. The most likely reason is that the NHC is violated when the vehicle turns around at a large heading rotation rate. Therefore, the proposed method is limited to land vehicular applications and is invalid for aviation applications, where the host carrier does not conform to NHC.

Comparing the results from the car, robot, and tractor tests, we notice that the proposed method has much better alignment accuracy for the car test than for both the robot and tractor applications, as shown in Figs. 5 and 6. The reasons may be as follows: 1) the car travels at higher speeds and travels over a longer distance within the same alignment period; 2) the percentage of time spent moving along a straight line by the car is larger than that of the robot ground vehicle tests; and 3) the motion of the car meets the NHC better than that of the other two carriers. The robot and tractor

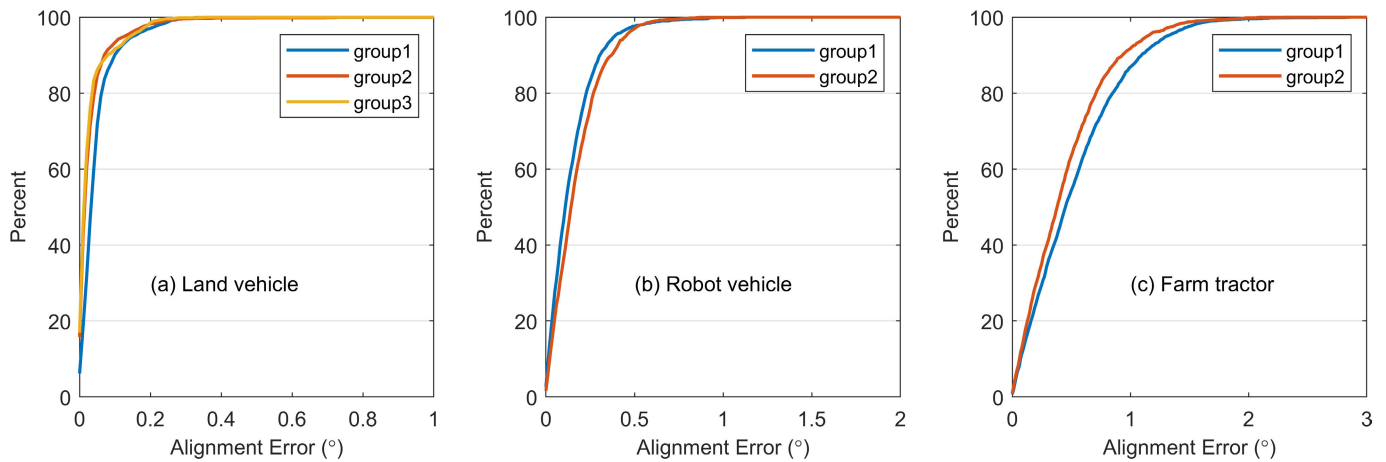


Fig. 6. CDF plots of the initial heading alignment errors on different carriers (the alignment period is 5 s). (a) Land vehicle. (b) Robot vehicle. (c) Farm tractor.

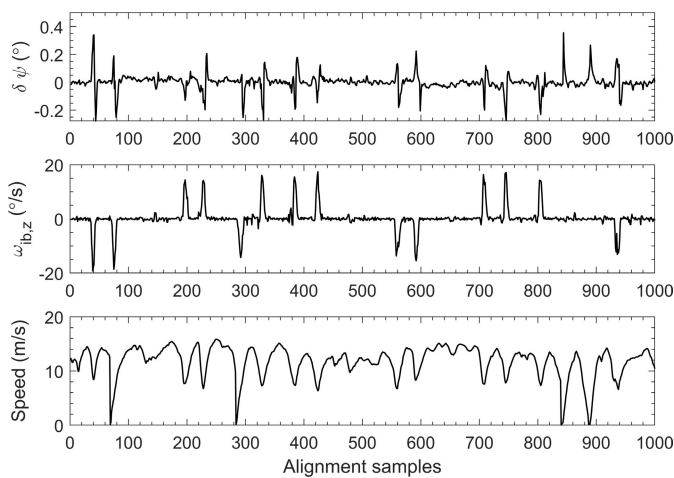


Fig. 7. Correlations of the heading alignment error with the vehicle steering rate and speed.

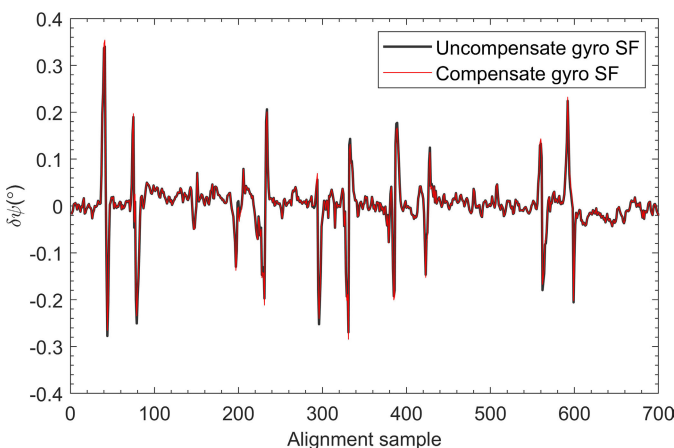


Fig. 8. Influence of the gyro scale factor error on the alignment accuracy.

both travel at almost the same low speed, and the tractor does not frequently change its heading, though the heading alignment error in the tractor application is still larger than that in the robot application, as depicted in Fig. 6. The most

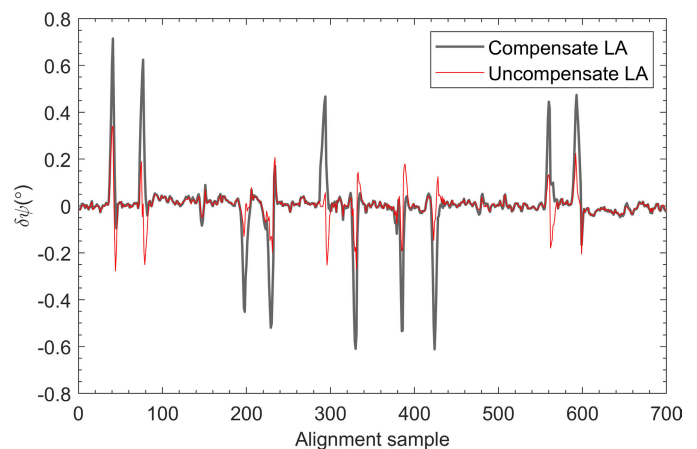


Fig. 9. Influence of the NHC LA compensation on the alignment accuracy.

likely explanation is that the tractor moves on muddy land and may slide slightly in the lateral direction, thus violating the NHC condition. It is not possible for us to quantitatively evaluate how the NHC's influences the alignment accuracy. On the other hand, we should state that even in this "worst condition," the proposed alignment method achieves much better alignment performance than previous research in both accuracy and time efficiency.

In common land vehicular applications, accurate RTK positions are not always available. We evaluated the proposed method using IMU data from group 1 of the land vehicles but processed the GNSS data in SPP mode. It also performs well, but the accuracy is degraded from 0.25° (RTK mode) to 4.7° at a 98.6% confidence level. If we extend the alignment period to 20 s, the initial heading can be determined with an accuracy of 1.6° at a 98.6% confidence level, as shown in Fig. 10, which is also better than most of the conventional alignment methods.

Based on the discussion above, to achieve the best performance of the proposed method, we have the following suggestions.

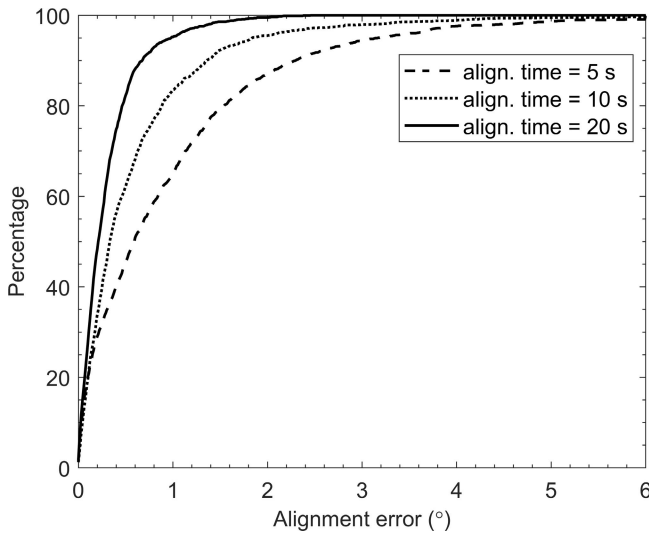


Fig. 10. CDF plots of the initial heading alignment errors of the INS aided by the GNSS SPP solution in the car test.

- 1) The straight-line course without a significant heading rotation rate is the best for carrying out the operation alignment.
- 2) The host vehicle is suggested to move as far as possible in the alignment stage to enlarge the travel distance.
- 3) The IMU mounting angles and the NHC LA should be calibrated or measured carefully in advance.

V. CONCLUSION

The land vehicular MEMS GNSS/INS-integrated systems face the challenge of rapid and accurate initial heading alignment. In this research, we proposed a method that determines the initial heading through matching the trajectories from DR and the GNSS. The DR trajectory is computed through a DR calculator using the gyro-derived attitude solution and the travel distance measured with the GNSS without using the accelerometer triads, and the GNSS trajectory is provided readily by the GNSS positioning algorithm. We prove that in a short period, the DR trajectory is similar in shape but has a rotation with respect to the true trajectory; then, the initial INS heading is determined from the angle bias between the inertial-based DR-indicated trajectory and the GNSS-indicated trajectory. Compared with the conventional in-motion alignment methods, the proposed algorithm has advantages in both time efficiency and accuracy and imposes fewer requirements on the host vehicle's motion.

APPENDIX

The errors in the gyro-derived attitude matrix $\hat{\mathbf{C}}_{b(t)}^{b(0)}$ mainly come from the gyro measurement errors, including the biases, scale factor error, cross-axis error, and random noise. The total angular rate measurement errors are modeled as follows:

$$\delta\boldsymbol{\omega} = \mathbf{b}_\omega + \mathbf{S}_\omega\boldsymbol{\omega} + \mathbf{N}_\omega\boldsymbol{\omega} + \boldsymbol{\varepsilon}_\omega \quad (\text{A.1})$$

where $\boldsymbol{\omega}$ is the true angular rate vector sensed by the gyroscope; \mathbf{b}_ω is the gyro bias vector; \mathbf{S}_ω is the scale factor error matrix; \mathbf{N}_ω is the cross-coupling matrix; and $\boldsymbol{\varepsilon}_\omega$ is the random measurement noise vector.

A. Random Noise

It is common to specify the random noise using the angular random walk (ARW), and the standard deviation of the ensuing attitude error, denoted by $\sigma(\delta\psi_{b,\varepsilon})$, is computed as follows [10, p. 207]:

$$\sigma(\delta\psi_{b,\varepsilon}) = \text{ARW} \cdot \sqrt{t}. \quad (\text{A.2})$$

The low-cost IMU used in our tests has the ARW of $0.12^\circ/\sqrt{h}$, as listed in Table II. The resulting attitude drift is $\sigma(\delta\psi_{b,\varepsilon}) = 0.12 \cdot \sqrt{5/3600} \approx 0.0045^\circ$ during the 5-s alignment period. Thus, the impact of the random noise on the gyro-derived attitude is negligibly small.

B. Fixed Gyro Bias

A fixed gyro bias produces an approximately linear attitude drift within a short time as follows:

$$\delta\boldsymbol{\psi}_{b,gb} = \mathbf{b}_\omega t \quad (\text{A.3})$$

where $\delta\boldsymbol{\psi}_{b,gb}$ is the attitude drift caused by a fixed gyro bias.

In practice, the large fixed gyro bias could be initially estimated by averaging the gyro measurements when the IMU remains stationary. Considering the residual impact of the random noise plus the ignored Earth rotation rate, the gyro bias could be estimated to the level of $18^\circ/h$ [8]. Therefore, the attitude drift induced by the gyro bias does not exceed 0.02° according to (A.3) when the alignment is accomplished within 5 s, which is negligibly small.

C. Scale Factor Error and Cross Coupling

The typical industrial MEMS IMUs usually exhibit a scale factor and cross-coupling errors up to 0.5%, as listed in Table II. For the land vehicle, the changes of the roll and pitch angle are usually small; thus, the impact of the cross coupling is negligibly small. The gyro scale factor error produces a heading error, denoted by $\delta\boldsymbol{\psi}_{b,sf}$, proportional to the heading change, denoted by $\Delta\boldsymbol{\psi}_t$, during the alignment

$$\delta\boldsymbol{\psi}_{b,sf} = S_\omega \Delta\boldsymbol{\psi}_t \quad (\text{A.4})$$

where S_ω is the gyro's scale factor error. The gyro scale factor and cross-coupling error cannot be estimated in real time within a short period of time during alignment due to the lack of observability. Thus, we have to accept these errors at full magnitude. Suppose that in the worst cases, the vehicle turns an angle of 50° (empirical value from car test experiments) during alignment; then, the gyro-derived heading error due to the gyro scale factor error is $50 \times 0.5\% = 0.25^\circ$. It is much smaller compared with the error of the given initial heading. In general, the scale factor error affects only the gyro-derived attitude solution when the vehicle turns around.

REFERENCES

- [1] S. Han and J. Wang, "A novel initial alignment scheme for low-cost INS aided by GPS for land vehicle applications," *J. Navigat.*, vol. 63, no. 4, pp. 663–680, Sep. 2010.
- [2] Z. F. Syed, P. Aggarwal, X. Niu, and N. El-Sheimy, "Civilian vehicle navigation: Required alignment of the inertial sensors for acceptable navigation accuracies," *IEEE Trans. Veh. Technol.*, vol. 57, no. 6, pp. 3402–3412, Nov. 2008.

- [3] E.-H. Shin and N. El-Sheimy, "An unscented Kalman filter for in-motion alignment of low-cost IMUs," in *Proc. Position Location Navigat. Symp. (PLANS)*, 2004, pp. 273–279.
- [4] L. Chang and B. Hu, "Robust initial attitude alignment for SINS/DVL," *IEEE/ASME Trans. Mechatronics*, vol. 23, no. 4, pp. 2016–2021, Aug. 2018.
- [5] X. Xu, Y. Sun, J. Gui, Y. Yao, and T. Zhang, "A fast robust in-motion alignment method for SINS with DVL aided," *IEEE Trans. Veh. Technol.*, vol. 69, no. 4, pp. 3816–3827, Apr. 2020.
- [6] Y. Huang, Y. Zhang, and X. Wang, "Kalman-filtering-based in-motion coarse alignment for odometer-aided SINS," *IEEE Trans. Instrum. Meas.*, vol. 66, no. 12, pp. 3364–3377, Dec. 2017.
- [7] P. D. Groves, R. J. Handley, and S. T. Parker, "Vehicle heading determination using only single-antenna GPS and a single gyro," in *Proc. 22nd Int. Tech. Meeting Satell. Division Inst. Navigat. (ION GNSS)*, 2009, pp. 1775–1784.
- [8] Q. Chen, H. Lin, R. Guo, and X. Niu, "Rapid and accurate initial alignment of the low-cost MEMS IMU chip dedicated for tilted RTK receiver," *GPS Solutions*, vol. 24, no. 4, pp. 1–13, Oct. 2020.
- [9] R. Sun, Q. Cheng, and J. Wang, "Precise vehicle dynamic heading and pitch angle estimation using time-differenced measurements from a single GNSS antenna," *GPS Solutions*, vol. 24, no. 3, pp. 1–9, Jul. 2020.
- [10] P. D. Groves, *Principles of GNSS, Inertial, and Multisensor Integrated Navigation Systems*, 2nd ed. Boston, MA, USA: Artech House, 2013.
- [11] R. M. Rogers, "IMU in-motion alignment without benefit of attitude initialization," *Navigation*, vol. 44, no. 3, pp. 301–311, Sep. 1997.
- [12] R. M. Rogers, *Applied Mathematics in Integrated Navigation Systems*, vol. 1, 3rd ed. Reston, VA, USA: AIAA, 2007.
- [13] H. S. Hong, J. G. Lee, and C. G. Park, "Performance improvement of in-flight alignment for autonomous vehicle under large initial heading error," *IEE Proc., Radar, Sonar Navigat.*, vol. 151, no. 1, pp. 57–62, Feb. 2004.
- [14] D. Wang, H. Lv, and J. Wu, "In-flight initial alignment for small UAV MEMS-based navigation via adaptive unscented Kalman filtering approach," *Aerosp. Sci. Technol.*, vol. 61, pp. 73–84, Feb. 2017.
- [15] M. Wu, Y. Wu, X. Hu, and D. Hu, "Optimization-based alignment for inertial navigation systems: Theory and algorithm," *Aerosp. Sci. Technol.*, vol. 15, no. 1, pp. 1–17, Jan./Feb. 2011.
- [16] Y. Wu and X. Pan, "Velocity/position integration formula. Part I: Application to in-flight coarse alignment," *IEEE Trans. Aerosp. Electron. Syst.*, vol. 49, no. 2, pp. 1006–1023, Apr. 2013.
- [17] Y. Wu, J. Wang, and D. Hu, "A new technique for INS/GNSS attitude and parameter estimation using online optimization," *IEEE Trans. Signal Process.*, vol. 62, no. 10, pp. 2642–2655, May 2014.
- [18] Y. Wei, H. Li, and M. Lu, "Carrier Doppler-based initial alignment for MEMS IMU/GNSS integrated system under low satellite visibility," *GPS Solutions*, vol. 25, no. 3, pp. 1–11, Jul. 2021.
- [19] L. Chang, J. Li, and K. Li, "Optimization-based alignment for strapdown inertial navigation system: Comparison and extension," *IEEE Trans. Aerosp. Electron. Syst.*, vol. 52, no. 4, pp. 1697–1713, Aug. 2016.
- [20] Y. Huang, Y. Zhang, and L. Chang, "A new fast in-motion coarse alignment method for GPS-aided low-cost SINS," *IEEE/ASME Trans. Mechatronics*, vol. 23, no. 3, pp. 1303–1313, Jun. 2018.
- [21] Y. Huang, Z. Zhang, S. Du, Y. Li, and Y. Zhang, "A high-accuracy GPS-aided coarse alignment method for MEMS-based SINS," *IEEE Trans. Instrum. Meas.*, vol. 69, no. 10, pp. 7914–7932, Oct. 2020.
- [22] Q. Zhang, S. Li, Z. Xu, and X. Niu, "Velocity-based optimization-based alignment (VBOBA) of low-end MEMS IMU/GNSS for low dynamic applications," *IEEE Sensors J.*, vol. 20, no. 10, pp. 5527–5539, May 2020.
- [23] S. de La Parra and J. Angel, "Low cost navigation system for UAV's," *Aerosp. Sci. Technol.*, vol. 9, no. 6, pp. 504–516, 2005.
- [24] G. Dissanayake, S. Sukkarieh, E. Nebot, and H. Durrant-Whyte, "The aiding of a low-cost strapdown inertial measurement unit using vehicle model constraints for land vehicle applications," *IEEE Trans. Robot. Autom.*, vol. 17, no. 5, pp. 731–747, Oct. 2001.
- [25] Q. Chen, Q. Zhang, and X. Niu, "Estimate the pitch and heading mounting angles of the IMU for land vehicular GNSS/INS integrated system," *IEEE Trans. Intell. Transp. Syst.*, vol. 22, no. 10, pp. 6503–6515, Oct. 2021.
- [26] P. Savage, "Strapdown inertial navigation integration algorithm design. Part 1: Attitude algorithms," *J. Guid., Control Dyn.*, vol. 21, no. 1, pp. 19–28, 1998.
- [27] P. G. Savage, *Strapdown Analytics—Part 1*. Maple Plain, MN, USA, 2007.
- [28] X. Niu et al., "Using Allan variance to analyze the error characteristics of GNSS positioning," *GPS Solutions*, vol. 18, no. 2, pp. 231–242, Apr. 2014.



Qijin Chen received the B.Eng. and Ph.D. degrees in geodesy and survey engineering from Wuhan University, Wuhan, China, in 2011 and 2016, respectively.

He is currently an Associate Research Fellow with the GNSS Research Center, Wuhan University. His research interests include inertial navigation system (INS) with aiding and its applications in geodesy and precise surveying engineering, including railway track geometry measuring and underground pipeline surveying.



Huan Lin received the B.E. degree in geodesy and survey engineering from Wuhan University, Wuhan, China, in 2019, where she is currently pursuing the master's degree with the GNSS Research Center.



Jian Kuang received the B.Eng. and Ph.D. degrees in geodesy and survey engineering from Wuhan University, Wuhan, China, in 2013 and 2019, respectively.

He is currently a Postdoctoral Fellow with the GNSS Research Center, Wuhan University. His research interests include inertial navigation, pedestrian navigation, and indoor positioning.



Yarong Luo received the B.Eng. degree in space science and technology from Xidian University, Xi'an, China, in 2016. He is currently pursuing the Ph.D. degree with the GNSS Research Center, Wuhan University, Wuhan, China, under the instruction of Jingnan Liu.

His research interests include nonlinear geometric filtering, data fusion, and global navigation satellite system (GNSS)/inertial navigation system (INS) integration for vehicle navigation. He has been focusing on unmanned system navigation.



Xiaoji Niu received the bachelor's and Ph.D. degrees from the Department of Precision Instruments, Tsinghua University, Beijing, China, in 1997 and 2002, respectively.

He did his postdoctoral research at the University of Calgary, Calgary, AB, Canada. He has worked as the Senior Scientist of SiRF Technology Inc., Shanghai, China. He is now a Professor with the GNSS Research Center, Wuhan University, Wuhan, China. He leads a multisensor navigation group focuses on global navigation satellite system (GNSS)/inertial navigation system (INS) integrations, low-cost navigation sensor fusion, and its new applications. He has published more than 90 academic articles and own 28 patents.